

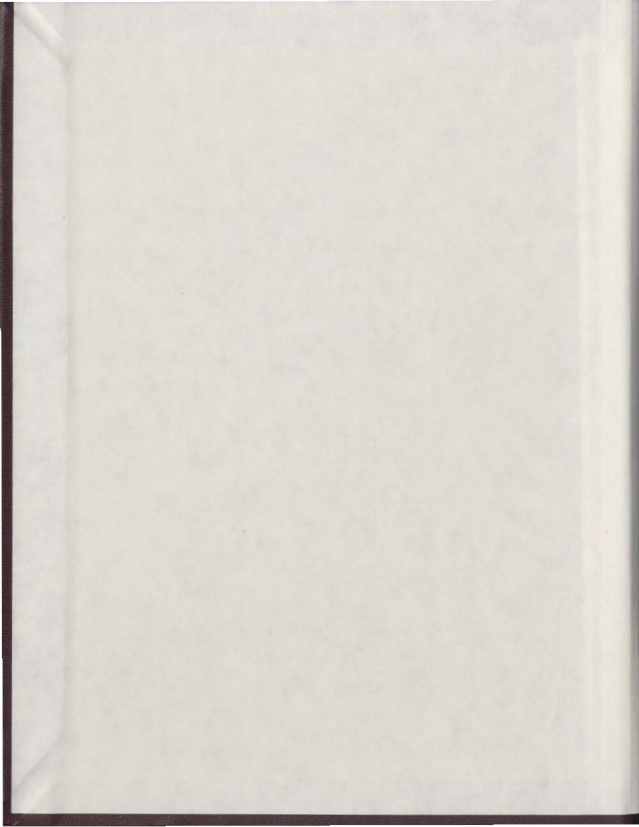
SIMULTANEOUS DETERMINATION OF COMPRESSIONAL
AND SHEAR ELASTIC WAVE VELOCITIES IN
CANADIAN EAST COAST SEDIMENTARY ROCKS AS
FUNCTIONS OF PRESSURE AND TEMPERATURE

CENTRE FOR NEWFOUNDLAND STUDIES

**TOTAL OF 10 PAGES ONLY
MAY BE XEROXED**

(Without Author's Permission)

[[ROBERT E. GAGNON]]



007147





CANADIAN THESES ON MICROFICHE

I.S.B.N.

THESES CANADIENNES SUR MICROFICHE



National Library of Canada
Collections Development Branch

Canadian Theses on
Microfiche Service

Ottawa, Canada
K1A 0N4

Bibliothèque nationale du Canada
Direction du développement des collections

Service des thèses canadiennes
sur microfiches

NOTICE

The quality of this microfiche is heavily dependent upon the quality of the original thesis submitted for microfilming. Every effort has been made to ensure the highest quality of reproduction possible.

If pages are missing, contact the university which granted the degree.

Some pages may have indistinct print especially if the original pages were typed with a poor typewriter ribbon or if the university sent us a poor photocopy.

Previously copyrighted materials (journal articles, published tests, etc.) are not filmed.

Reproduction in full or in part of this film is governed by the Canadian Copyright Act, R.S.C. 1970, c. C-30. Please read the authorization forms which accompany this thesis.

THIS DISSERTATION
HAS BEEN MICROFILMED
EXACTLY AS RECEIVED

AVIS

La qualité de cette microfiche dépend grandement de la qualité de la thèse soumise au microfilmage. Nous avons tout fait pour assurer une qualité supérieure de reproduction.

S'il manque des pages, veuillez communiquer avec l'université qui a conféré le grade.

La qualité d'impression de certaines pages peut laisser à désirer, surtout si les pages originales ont été dactylographiées à l'aide d'un ruban usé ou si l'université nous a fait parvenir une photocopie de mauvaise qualité.

Les documents qui font déjà l'objet d'un droit d'auteur (articles de revue, examens publiés, etc.) ne sont pas microfilmés.

La reproduction, même partielle, de ce microfilm est soumise à la Loi canadienne sur le droit d'auteur, SRC 1970, c. C-30. Veuillez prendre connaissance des formules d'autorisation qui accompagnent cette thèse.

LA THÈSE A ÉTÉ
MICROFILMÉE TELLE QUE
NOUS L'AVONS REÇUE

SIMULTANEOUS DETERMINATION OF COMPRESSIONAL AND
SHEAR ELASTIC WAVE VELOCITIES IN CANADIAN EAST
COAST SEDIMENTARY ROCKS AS FUNCTIONS OF PRESSURE
AND TEMPERATURE.

by



Robert E. Gagnon, BSc.

Submitted in partial fulfilment
of the requirements of the degree of
Master of Science

Memorial University of Newfoundland

August, 1981

To Namazu-e

- 1 -

CONTENTS

	<u>PAGE</u>
ABSTRACT	111
LIST OF TABLES	iv
LIST OF FIGURES AND ILLUSTRATIONS	v
CHAPTER I:	
1. Introduction	1
2. Velocity Techniques	2
3. Results of Previous Studies	4
(a) Hysteresis	4
(b) Saturation	5
(c) Anisotropy	6
(d) Present Study	7
CHAPTER II:	
1. Theory	8
(a) Non-porous Solids	8
(b) Porous Solids	11
CHAPTER III:	
1. Apparatus	16
(a) Transducer Design and Travel Time Measurements	16
(b) Acoustic Coupling and Offset Determination	25
(c) Heating Jacket	29
2. Preparation and Jacketing of Samples and Measurement Procedure	31
CHAPTER IV:	
1. Results and Discussion	33
(a) Anisotropy and Hysteresis	36
(b) Note on Polarization Effects	57
(c) Effects of Saturation	57

	<u>PAGE</u>
CHAPTER IV: 1. Results and Discussion (Cont'd)	
(d) Comparison With in Situ Well Logs	70
(e) Temperature Effects	72
CHAPTER V: 1. Summary	75
REFERENCES	79
ACKNOWLEDGEMENTS	82

ABSTRACT

An apparatus has been designed and constructed to determine accurately, using the pulse transmission method, compressional ($\pm 1\%$) and shear ($\pm 2\%$) wave velocities as functions of temperature and pressure. A significant feature of the design, made possible by stacking the piezoelectric transmitting and receiving P and S-wave transducers, is the ability to measure both shear and compressional velocities with each experiment. The device has been employed to study sedimentary core samples taken from wells on the Labrador Shelf and the Grand Banks of Newfoundland. With a few exceptions the results show qualitative agreement with Biot's theory for propagation of elastic waves through porous solids. Comparison with well log velocities, however, shows significant discrepancies which arise for several reasons.

Velocity anisotropy has been observed between samples taken parallel and perpendicular to the bedding plane. The most extreme case exhibited an anisotropic effect of 10%. The dominant mechanisms proposed to explain anisotropy are crack and pore alignment and inhomogeneous distribution of rock constituents.

The effect of temperature is found to be small compared with the influence of hydrostatic pressure. A 40°C change in temperature in the range studied ($7^{\circ}\text{C} - 90^{\circ}\text{C}$) does not affect velocities by more than 2%.

LIST OF TABLES

		<u>PAGE</u>
Table 1	Instrumentation and Manufacturers	18
Table 2	Locations, Properties and Descriptions of Samples	35
Table 3	Vp and Vs Values for Cormorant N-83 8of8 Samples	37
Table 4	Vp and Vs Values for Cormorant N-83 6of8 Samples and Cormorant N-83 6of8 Samples	38
Table 5	Vp and Vs Values for Cormorant N-83 6of8 Samples	39
Table 6	Vp and Vs Values for Coot K-56-4of5 (1) and Vp Values for Cormorant N-83 7of8 (1)	40
Table 7	Vp and Vs Values for Herjolif M-92 Samples	41
Table 8	Well Log Vp Compared With Laboratory Measurements	71

LIST OF FIGURES AND ILLUSTRATIONS

	PAGE
Figure 1 Pressure Vessel and Transducer Assembly	17
Figure 2 Examples of Compressional and Shear Wave Signals	20
Figure 3 Photograph of Jacketed Rock Sample and Endplugs	21
Figure 4 Block Diagram of the Complete System Used for Velocity Determinations	23
Figure 5 Photograph of Pressure Gauge and Electrical Instrumentation	24
Figure 6 Photograph of Heating Jacket	30
Figure 7 Map Showing Well Sites	34
Figure 8-9	42-43
10-12	44-46
13-20	Graphic Juxtapositions of the
21-25	Velocity Data From Tables (3-7)
26-31	58-62
32-33	64-69
	73-74
Figure 34 Magnified Side Wall Views of Cormorant N-83 8of8 and Cormorant N-83 6of8	77

CHAPTER I

1. Introduction

In the fields of petroleum and geological engineering and geophysics considerable interest is given to determining compressional and shear wave velocities and attenuation in fluid saturated and dry sedimentary rocks. The three main parameters that affect the attenuation and velocities are overburden and pore fluid pressures, the type of saturant, and the degree of solid matrix anisotropy. As examples, geological engineers who choose sites for large structures need to know the influence of water saturation and pore pressure on the strength and elastic moduli. Mechanisms of drilling (and blasting) can be better understood by determining dynamic elastic moduli from velocity measurements. Correct interpretation of earth structures as derived from seismic records must incorporate knowledge of how confining pressure affects wave velocities. Christensen *et al.* (1973) showed that it is possible to derive the structure of ocean floor layering by using the differing linear relationships between V_p and V_s for sedimentary and basaltic rock. In order to use acoustic velocity log records effectively, the petroleum industry requires detailed knowledge of how velocities are affected by porosity, changes in rock bulk compressibility and fluid saturation of sedimentary rocks. These indicate a few

applications of velocity measurements in the laboratory where parameters that affect the velocity can be independently controlled and monitored.

2. Velocity Techniques

The earliest laboratory studies of seismic velocities employed the pulse transmission method, whereby ultrasonic transducers were used to send and receive a pulse of acoustic energy through a given rock sample. An oscilloscope was used to compare the received signal with a similar pulse which had travelled through a mercury column of adjustable length. The compressional wave velocity for mercury is well known so the travel time through the mercury and hence through the rock sample could be obtained. The method for determining compressional wave velocities has been developed by Hughes and Cross (1951), Wyllie et al. (1956) and Birch (1960) using axially polarized or X-cut quartz piezoelectric crystals as transducers. Ultrasonic frequencies are typically in the MHz range whereas real earth and exploratory seismic events have periods of the order of .1 sec.

Shear wave velocities have been measured at atmospheric pressure using first arrival methods developed by Peselnick and Zietz (1959) and Peselnick (1962). AC-cut transducers were used for these measurements. Simmons (1964) was able to determine shear velocities in rocks at confining pressures up to 10 kilobars (1GPa). King (1966), instead of using shear wave generating ceramic transducers, used a compressional transducer to generate shear waves

by mode conversion at a free surface.

Studies have also been done using the resonant bar technique. In this case a rock sample is forced to vibrate in one of several normal modes at the associated resonant frequency. There exist fairly simple relationships between resonant frequencies and elastic wave velocities for homogeneous isotropic materials. This method was used by Gardner *et al.* (1964) to determine attenuation of elastic waves as a function of confining pressure and various fluid saturants. Difficulties which require corrections are encountered if anisotropic specimens are to be studied. Corrections also have to be made to account for the effect of the jacket around the sample and the frictional effects of the fluid on the specimen due to confining pressure.

Another technique used to determine shear and compressional wave velocities is the critical angle method. King and Fatt (1962) used barium titanate transducers to cause a parallel beam of ultrasonic energy to impinge, via a liquid filled bath, on one face of a parallel sided rock sample which was free to rotate about an axis perpendicular to the beam in the liquid. A second transducer situated on the opposite side of the sample and located on the axis of the beam picked up any transmitted energy. The laws of optics for reflection and refraction at boundaries of different media can be used, along with the known velocity of sound in the liquid and the angles at which minima appear in transmitted energy, to determine V_s and V_p for the rock sample. This method, however,

does have certain limitations. A narrow beam requires a high frequency source, but the wavelength is restricted by the largest grain or pore size of the rock. In practise, it is only when the sample is of a certain optimum thickness, which depends on the shear wavelength in the material and the refracted shear wave angle at the critical angle for compressional waves, that compressional wave minima can be readily detected. Also, the observed minima in transmitted intensity are not sharp enough to give velocity accuracies as good as some other methods which typically range from .3% to 2% for P-waves and .5% to 10% for S-waves.

3. Results of previous studies

(a) Hysteresis

With regard to the results of earlier studies one phenomenon constantly referred to in the literature is that of hysteresis. That is, at a certain point in the pressure temperature path the velocity seems to be dependent to some extent on the path taken to that temperature and pressure. Birch (1960) and Gardner et al. (1965) showed that for a given temperature, the velocity along a path of decreasing pressure is generally higher than the velocity along a path of increasing pressure. For dry Franciscan rocks at higher temperatures, hysteresis appears to be less pronounced and the velocity pressure curve is more linear. Furthermore, it seems that linearity of the pressure velocity curve and subdued hysteresis remain when the temperature

is lowered, as was observed by Stewart and Peselnick (1977). They and others (Hughes and Jones (1951)) also noticed that small increases of velocity occur with all pressures at low temperatures after completion of a high temperature cycle. O'Connell and Budiansky (1974) showed that hysteresis can be attributed to cracks in the rocks and their configuration which would give rise to variations of bulk elastic moduli. Buessem (1961) showed that crack or grain boundary sliding due to locally non-hydrostatic stress or from recombination phenomena, can cause hysteresis in crack configuration. Differential thermal expansion may result in the closure of cracks which have remained open under applied pressure alone. These cracks which have been closed by thermal expansion could conceivably remain closed, in part at least, when the rocks are cooled, thus resulting in higher velocities at a lower temperature than had been observed before the heating took place. Cracks which close at elevated temperatures may have been caused by cooling as the rocks come to the surface. Thermal and stress history may be determined from velocity and hysteresis behaviour (Stewart and Peselnick (1977)).

(b) Saturation

In general Hughes and Cross (1951), Wyllie et al. (1956), and Hughes and Kelly (1952) have shown that the effects of complete saturation of porous rocks vary strongly with confining pressure when zero pore pressure is maintained. Upon saturation, compressional wave velocities increase at low confining pressures. Wyllie

et al. (1962) and other authors report an increase in shear wave velocity with saturation while Jones and Wang (1981) and Toksöz et al. (1979) report a decrease. King (1966) noted both conditions in the same specimen, that is, saturated velocities higher than dry velocities for low confining pressures and the opposite situation at higher pressures. In general the more recent, and perhaps more reliable experimental data is in qualitative agreement with Biot's (1962) predicted decrease in shear wave velocity with saturation. Other experiments have shown that elastic wave velocities are a function of the difference between pore and confining pressure. Wyllie et al. (1958) and King (1966) found that compressional waves have velocities that remain constant for constant differential pressure. Desai et al. (1969) and Hughes and Cross (1951) have found that the effect of constant differential pressure on velocity is to cause the rocks to behave similar to dry rocks at high pressure.

(c) Anisotropy

Velocity anisotropy has been studied by a few authors. Stewart and Peselnick (1977) noticed small effects in some of the Franciscan rocks they investigated: 1 - 3% in one case and in another it was found that anisotropy became more pronounced with temperature though the effect was small, 0 - 1%. Carlson and Christensen (1979) noticed significant degrees of anisotropy (between 5% and 16%) for compressional waves in semi-indurated calcareous deep sea sediments. A detailed account of possible

reasons for anisotropy will be discussed later in relation to my own results. Briefly the effect is related to preferred crack and pore orientation, inhomogeneous distribution and orientation of rock constituents, and selective orientation of anisotropic crystals such as calcite.

(d) Present study

The purpose of the present study is to design and construct an apparatus capable of shear and compressional velocity determinations and to use it on a limited set of sedimentary rocks (8) to investigate 1. the effect of pressure and temperature on seismic velocities, 2. the presence of anisotropy between vertical drill core samples (I) taken perpendicular to the plane of the bedding and transverse samples (II) taken parallel to the bedding plane, and how such anisotropy is affected by pressure, 3. Biot's (1962) theory for dry and saturated solids, 4. velocity results using bore-hole techniques as compared with laboratory measurements.

A few samples, rather than a broad sweep of bore-hole sections, have been used because there are significant results peculiar to short sections of rock which would not necessarily show up in a statistically averaged study of much larger sections. Also it is difficult to obtain evenly spaced core samples of a suitable quality for large sections.

The core samples come from three holes in Eastern Canada. Two holes are on the Grand Banks of Newfoundland and the other is on the Labrador Shelf.

strain components respectively, we have the general relation

$$V_{elastic} = \frac{1}{2} \sigma_{ik} \epsilon_{ik} \quad (3)$$

where we have adopted the double indice summation convention.

For linear elasticity, the factors σ_{ik} are linear functions of the ϵ_{ik} 's

$$\sigma_{ik} = C_{iklmn} \epsilon_{mn} \quad (4)$$

Here the elastic constants of the material are given by C_{iklmn} .

Fortunately, these constants which linearly relate stress and strain can be reduced to only two for homogeneous isotropic non-porous media. On the scale of wave-lengths usually employed in seismological problems microscopic anisotropy is much smaller and the bulk-solid may be considered isotropic. The following notation simplifies further derivation

$$(x, y, z) \equiv (x_1, x_2, x_3) \quad (5)$$

$$(\xi, \eta, \zeta) \equiv (d_1, d_2, d_3)$$

$$\delta_{ij} = \begin{cases} 1 & i=j \\ 0 & i \neq j \end{cases} \quad (6)$$

The strains ϵ_{ij} can now be written as

$$\epsilon_{ij} = \frac{1}{2} \left(\frac{\partial d_i}{\partial x_j} + \frac{\partial d_j}{\partial x_i} \right) \quad (7)$$

so that the volume dilatation is

$$\epsilon = \frac{\partial d_1}{\partial x_1} + \frac{\partial d_2}{\partial x_2} + \frac{\partial d_3}{\partial x_3} = \xi_x + \eta_y + \zeta_z \quad (8)$$

where the subscripts x, y, z indicate partial derivatives.

For the isotropic case, according to Hooke's Law, the stresses as linear functions of the strains are written

$$\sigma_{ij} = \lambda E \delta_{ij} + 2\mu E_{ij} \quad (9)$$

where μ , the rigidity, and λ are the Lamé constants of the solid.

The constant $\nu = \frac{\lambda}{2(\lambda + \mu)}$ is known as Poisson's Ratio.

Reducing the treatment to two dimensions and assuming homogeneity in the x, y directions enables us to write the Lagrangian as

$$L = T - V_{elastic} \quad (10)$$

where the elastic potential energy density is

$$V_{elastic} = \frac{1}{2} [(\lambda + 2\mu)(\xi_x^2 + \xi_z^2) + 2\lambda \xi_x \xi_z + \mu(\xi_z + \xi_x)^2 + \mu(\eta_x^2 + \eta_z^2)^2] \quad (11)$$

Application of the Euler-Lagrange equations will yield for the case of shear waves

$$\rho \ddot{\eta} = \frac{\partial}{\partial x} \mu \eta_x + \frac{\partial}{\partial z} \mu \eta_z \quad (12)$$

For constant rigidity μ we have simply

$$\rho \mu \ddot{\eta} = \nabla^2 \eta \quad (13)$$

i.e. a scalar wave equation with propagation velocity

$$v_s = \left(\frac{\mu}{\rho}\right)^{\frac{1}{2}} \quad (14)$$

For the case of compressional waves a similar treatment

yields the wave equation

$$\frac{1}{v_p^2} \ddot{\sigma} = \nabla^2 \sigma \quad (15)$$

where $\sigma = (\lambda + 2\mu)E$. Hence

$$v_p = \left(\frac{\lambda + 2\mu}{\rho}\right)^{\frac{1}{2}} \quad (16)$$

(b) Porous Solids

For porous media we begin by assuming that macroscopically there is a uniform and isotropic distribution of small pores of arbitrary shape. The pore size is small compared to the wavelength of the propagating waves. When the pores are liquid filled, the average displacement vectors of the liquid and solid are $\vec{d}_2(\xi_2, \eta_2, \zeta_2)$ and $\vec{d}_1(\xi_1, \eta_1, \zeta_1)$ respectively.

We again confine ourselves, for simplicity, to the two-dimensional formalism used with non-porous solids.

For the theory to be linear the kinetic energy density must be a quadratic function of the velocities $\dot{\vec{d}}_1, \dot{\vec{d}}_2$ so that it can only have the form

$$\mathcal{T} = \frac{1}{2} \left[\rho_{11} (\dot{\xi}_1^2 + \dot{\zeta}_1^2) + 2\rho_{12} (\dot{\xi}_1 \dot{\xi}_2 + \dot{\zeta}_1 \dot{\zeta}_2) + \rho_{22} (\dot{\xi}_2^2 + \dot{\zeta}_2^2) \right] \quad (17)$$

which includes inertial coupling between the liquid fraction and the solid matrix. The quantities $\rho_{11}, \rho_{12}, \rho_{22}$ are given as

$$\begin{aligned} \rho_{11} &= \rho_1 + \rho_a \\ \rho_{12} &= -\rho_a \\ \rho_{22} &= \rho_2 + \rho_a \end{aligned} \quad (18)$$

where ρ_1 is the mass of solid per unit volume of the solid-plus-fluid aggregate and ρ_2 is the corresponding mass of fluid. ρ_a is the "apparent" mass due to the fluid. Birkhoff (1960) defined it as the difference between the inertia which a body has in a fluid and in vacuo.

A further consequence of linearity of theory is that stress and strain are linearly related.

In two dimensions we have

$$\sigma_{11} = 2M\epsilon_{11} + A\epsilon_1 + Q\epsilon_2 \quad (a)$$

$$\sigma_{33} = 2M\epsilon_{33} + A\epsilon_1 + Q\epsilon_2 \quad (b)$$

$$\sigma_{13} = 2M\epsilon_{13} \quad (c)$$

$$\sigma_2 = S\epsilon_1 + R\epsilon_2 \quad (d)$$

The ϵ_{ij} and σ_{ij} here, apply to the solid, and the divergences of the solid and fluid displacement fields \vec{d}_1, \vec{d}_2 are ϵ_1, ϵ_2 . The solid exerts a pressure σ_2 on the fluid. Due to assumed isotropy the coefficients Q and A will be the same in (19a) and (19b). The further requirement that the system be conservative and stable necessitates that $S = Q$.

The potential energy has the form

$$V_{elastic} = \frac{1}{2} (\sigma_{11} \epsilon_{11} + \sigma_{33} \epsilon_{33} + 2 \sigma_{13} \epsilon_{13} + \sigma_2 \epsilon_2) \quad (20)$$

Applying Lagrange's equations to $L = \mathcal{J} - V_{elastic}$, where \mathcal{J} and $V_{elastic}$ are given by (17) and (20), we obtain

$$\rho_{11} \ddot{\xi}_1 + \rho_{12} \ddot{\xi}_2 - \frac{\partial}{\partial x} (A + 2M) \xi_{1x} - \frac{\partial}{\partial x} A \xi_{2x} - \frac{\partial}{\partial x} Q \epsilon_2 - \frac{\partial}{\partial z} M (\xi_{1z} + \zeta_{1z}) = 0$$

$$\rho_{12} \ddot{\xi}_1 + \rho_{22} \ddot{\xi}_2 - \frac{\partial}{\partial x} Q \epsilon_1 - \frac{\partial}{\partial x} R \epsilon_2 = 0$$

(21)

$$\rho_{11} \ddot{\zeta}_1 + \rho_{12} \ddot{\zeta}_2 - \frac{\partial}{\partial z} (A + 2M) \zeta_{1z} - \frac{\partial}{\partial z} A \zeta_{2z} - \frac{\partial}{\partial z} Q \epsilon_2 - \frac{\partial}{\partial z} M (\xi_{1z} + \zeta_{1z}) = 0$$

$$\rho_{12} \ddot{\zeta}_1 + \rho_{22} \ddot{\zeta}_2 - \frac{\partial}{\partial z} Q \epsilon_1 - \frac{\partial}{\partial z} R \epsilon_2 = 0$$

This system can be reduced to four uncoupled equations if M, A, Q, R are assumed to be constants. Writing

$$\vec{O}_1 = \text{curl } \vec{d}_1 \quad (22)$$

$$\vec{O}_2 = \text{curl } \vec{d}_2$$

and

$$K = A + 2M \quad (23)$$

we get

$$\rho_{11} \ddot{\epsilon}_1 + \rho_{12} \ddot{\epsilon}_2 = \nabla^2 (K \epsilon_1 + Q \epsilon_2) \quad (a)$$

$$\rho_{12} \ddot{\epsilon}_1 + \rho_{22} \ddot{\epsilon}_2 = \nabla^2 (Q \epsilon_1 + R \epsilon_2) \quad (b)$$

$$\rho_{11} \ddot{\vec{O}}_1 + \rho_{12} \ddot{\vec{O}}_2 = \mu \nabla^2 \vec{O}_1 \quad (c)$$

$$\rho_{12} \ddot{\vec{O}}_1 + \rho_{22} \ddot{\vec{O}}_2 = 0 \quad (d)$$

The following shear wave equation can be obtained from (24 c, d) by eliminating $\ddot{\vec{O}}_2$

$$\mu \nabla^2 \vec{O}_1 = \rho_{11} \left(1 - \frac{\rho_{12}^2}{\rho_{11} \rho_{22}} \right) \ddot{\vec{O}}_1 \quad (25)$$

Hence the shear wave velocity is given by

$$V_s = \left[\frac{\mu}{\rho_{11} \left(1 - \frac{\rho_{12}^2}{\rho_{11} \rho_{22}} \right)} \right]^{1/2} \quad (26)$$

Thus it is clear that shear velocities are greater in porous material than in non-porous material of the same composition. Furthermore, for a given porous rock we would expect the shear velocity to be lower when the rock is saturated with some fluid (say water), than when it is dry.

Equations (24 a,b) refer to compressional waves. We expect two types of waves since there are two unknowns ϵ_1, ϵ_2 and two equations. For convenience we define the reference velocity V_c , obtained by setting $\epsilon_1 = \epsilon_2$, i.e. no relative motion between fluid and solid, and adding equations (24a) and (24b)

$$V_c^2 = \frac{H}{\rho} \quad (27)$$

here

$$H = K + R + Z Q$$

$$S = S_{11} + Z S_{12} + S_{22} \quad (28)$$

We can assume that the waves travel in the x direction and have harmonic solutions

$$\begin{aligned} \epsilon_1 &= B_1 e^{i(\alpha x - \omega t)} \\ \epsilon_2 &= B_2 e^{i(\alpha x - \omega t)} \end{aligned} \quad (29)$$

B_1 and B_2 are constants and the phase velocity is given by

$$v = \frac{\omega}{\alpha} \quad (30)$$

Redefining the various parameters

$$\begin{aligned} \beta_{11} &= \frac{K}{H} & \beta_{22} &= \frac{R}{H} & \beta_{12} &= \frac{Q}{H} \\ \gamma_{11} &= \frac{S_{11}}{S} & \gamma_{22} &= \frac{S_{22}}{S} & \gamma_{12} &= \frac{S_{12}}{S} \end{aligned} \quad (31)$$

and rewriting (24 a, b) to obtain two homogeneous equations and putting $z = \frac{v^2}{v_c^2}$

$$\begin{aligned} z (\gamma_{11} B_1 + \gamma_{12} B_2) &= \beta_{11} B_1 + \beta_{12} B_2 \\ z (\gamma_{12} B_1 + \gamma_{22} B_2) &= \beta_{12} B_1 + \beta_{22} B_2 \end{aligned} \quad (32)$$

We observe that the compatibility of these equations requires the determinant of the coefficients to be zero, i.e.

$$z^2 (\gamma_{11} \gamma_{22} - \gamma_{12}^2) - z (\beta_{11} \gamma_{22} + \beta_{22} \gamma_{11} - 2\beta_{12} \gamma_{12}) + (\beta_{11} \beta_{22} - \beta_{12}^2) = 0 \quad (33)$$

The equation will have two roots z_1, z_2 corresponding to two compressional waves denoted by first and second kind.

Liquid and solid move in phase for waves of the first kind and out of phase for waves of the second kind. The first kind has the higher velocity, $v_1 > v_2$

$$v_1^2 = v_c^2 z_1 \quad (34)$$

$$v_2^2 = v_c^2 z_2$$

If we denote the amplitudes associated with Z_1 , as $B_1^{(1)}, B_2^{(1)}$ and those for Z_2 as $B_1^{(2)}, B_2^{(2)}$ equation (32) can be used to derive

$$Z_1 = \frac{\beta_{11} B_1^{(1)^2} + 2\beta_{12} B_2^{(1)} B_1^{(1)} + \beta_{22} B_2^{(1)^2}}{\gamma_{11} B_1^{(1)^2} + 2\gamma_{12} B_1^{(1)} B_2^{(1)} + \gamma_{22} B_2^{(1)^2}} \quad (35)$$

In the experiments that follow we are concerned only with compressional waves of the first kind since these are the first arrivals.

Hence the velocity of compressional waves through porous media is

$$V_p = v_f = \left(\frac{k + R + 2Q}{\rho} \cdot Z_1 \right)^{1/2} \quad (36)$$

With no saturant present $Z = 1$. In the presence of a saturant $Z > 1$. Also, in the unsaturated condition $R, Q = 0$, otherwise $R, Q > 0$. When dealing with sedimentary rocks the increase in ρ with saturation will be small compared to the combined effect of corresponding changes in R, Q and Z_1 . The velocity of compressional waves in a porous material is expected then to increase with saturation.

Detailed knowledge of M, K, S_w, R, Q , and Z_1 is needed for quantitative comparison of laboratory velocities with theory. This, however, is beyond the scope of the present study so that any comparisons made in the discussion of results will be strictly qualitative.

CHAPTER III

1. Apparatus

(a) Transducer design and travel time measurement

The technique employed to determine seismic velocities for these experiments is the pulse transmission method. The apparatus, however, differs somewhat from the types previously mentioned. Instead of attaching either a set of P or S-wave transducers to the end faces of a given sample, both types are stacked on each face (Figure 1). A shear-wave ceramic is placed next to the rock and on top of that a P-wave ceramic. These ceramic transducers are 12.70 mm in diameter and 2.54 mm thick. The same stacking arrangement is used for transmitting and receiving pairs. The electronic attachments are such that the transmitting transducers are both fired simultaneously by placing a 60 volt pulse across two metallic surfaces with the ceramics in between. Hence, a P and S-wave are transmitted down the rock at the same time. According to Biot's Theory they are completely uncoupled at the frequencies used (1 MHz for P-waves and .5MHz for S-waves). This was verified by experiments using only P transducers or S transducers. At the receiver, the signal from either transducer can be displayed on the dual trace oscilloscope (Table 1) depending on which wave form one wants to examine. I found, as did King (1966), that the wave forms did not change

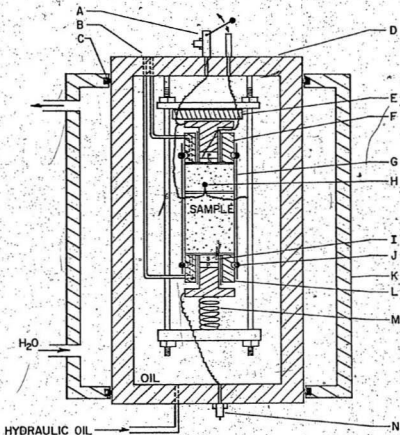


Figure 1. Pressure Vessel and Transducer Assembly. A. Electrical switch and connection for receiver transducer. B. Pore fluid passage tubes. C. O-ring seal between heating jacket and pressure vessel. D. Stainless steel pressure vessel (Table 1). E. Teflon electrical insulation between endplug and ground. F. Receiver transducer housing. G. Heat shrinkable flexible jacket. H. Bead resistance thermistor. I. Compression and shear wave generating ceramic crystals. J. O-ring which seals flexible jacket to endplug. K. Heating jacket. L. Transmitter transducer housing. M. Spring. N. Electrical connection for transmitting transducers.

TABLE 1
Model numbers and manufacturers of instrumentation

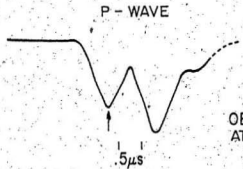
INSTRUMENT	MODEL #	MANUFACTURER
Unit Pulse AMI Unit Power Supply Unit Pulser	Type 1219A 1203 - A 1217 - A	General Radio Co. Cambridge Mass. USA
Function Generator	FG 501	Tektronix, Inc. Beaverton, Oregon
Universal Counter	DC 503	Tektronix
Dual Trace Oscilloscope	D 75	Tequipment, Division of Tektronix U.K. Ltd., London, England
Pressure Vessel	Model 41-14465	Aminco, Silver Spring, Maryland

appreciably for most rocks in the pressure range of these experiments. Therefore, all offsets and travel times are measured from the first negative peak of the wave forms (Figure 2). This virtually eliminates ambiguities which arise from trying to determine accurately first onsets, especially for the shear waves since these are always accompanied by a compressional wave precursor which greatly distorts the shear first onset.

The transducer holders are hollowed out cylinders of brass (Figures 1, 3) with a copper sheet silver soldered over one end. The copper sheet provides electrical contact for the ceramic transducers and is also a barrier between oil and the rock sample. Each of the brass endplugs has a small hole (≈ 7 mm diameter) drilled through the bottom providing access through the side where high pressure tubing has been silver soldered to the plug. These passages allow for the escape of pore fluid as the rock is compressed. The two ceramic transducers sit in a hollowed out portion of the brass plugs, with a solid brass cylinder on top of the ceramics. The inner cylinder is electrically insulated from the holder by a sleeve of heat shrinkable tubing. Positive and ground electrical connections are made with this inner plug and outer plug respectively, for the transmitting transducer assembly. The receiver endplug has basically the same arrangement with the added feature of a small insulated wire that runs between inner and outer brass cylinders and which makes electrical contact with a thin copper sheet conductor between the two piezoelectric ceramics.

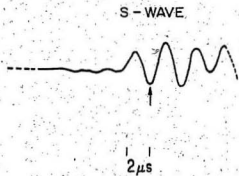
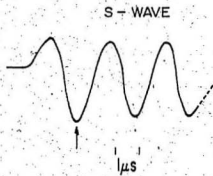
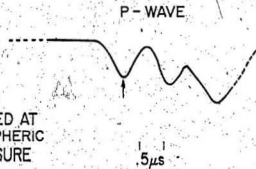
Figure 2. Examples of compressional and shear wave signals as they would appear on the oscilloscope screen.

END PLUGS FACE TO FACE



OBTAINED AT
ATMOSPHERIC
PRESSURE

CORMORANT 6 of 8 VERTICAL



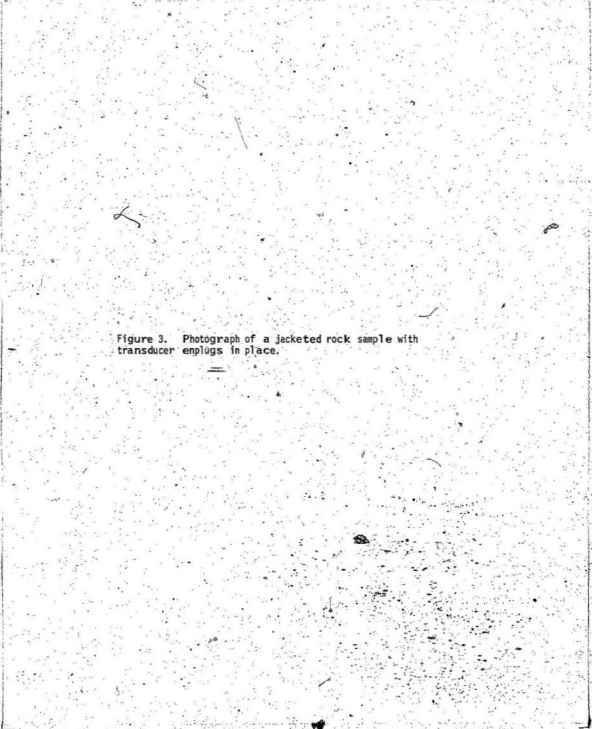


Figure 3. Photograph of a jacketed rock sample with transducer enplugs in place.



Faint handwritten text, possibly a date or reference number, located on the left margin of the page.

The two leads to the oscilloscope are always connected to the outer cylinder (i.e. the ground) and the inner cylinder. To view P-waves on the screen, the small wire lead between the ceramics is left open-circuited. For shear wave viewing this lead is shorted to the inner brass cylinder which effectively short-circuits any signal coming from the P-wave ceramic receiver. A mechanical switch is attached to the pressure vessel to facilitate this shorting procedure.

Accurate travel time measurements are made by employing a function generator (Table 1) capable of generating periodic shapes with periods as low as $\approx 7\mu\text{s}$ (Figures 4, 5). A square waveform, along with the seismic signal, is displayed on the dual trace oscilloscope and the function generator period is adjusted so that the negative going edge, which is used as the cursor, is lined up with whatever portion of the seismic signal measurements are to be taken from. A universal counter (Table 1) which can measure periods to within .1 ns is connected to the function generator and it registers the square wave period. This period, apart from a small offset correction due to electrical and mechanical delays in the system, corresponds to the acoustic travel time through the rock sample. In the present study we use the first negative peak of the seismic signal as the point from which travel time measurements are taken. This pulse generator (Table 1) and function generator are both synchronized by the internal trigger of the oscilloscope. The accuracy of the

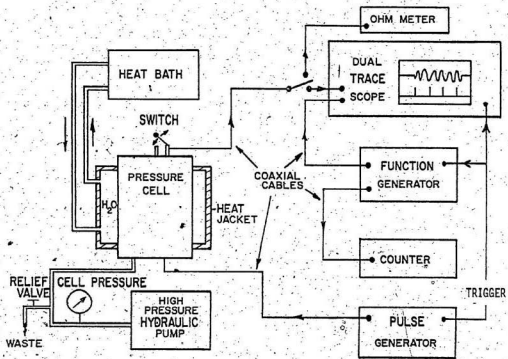
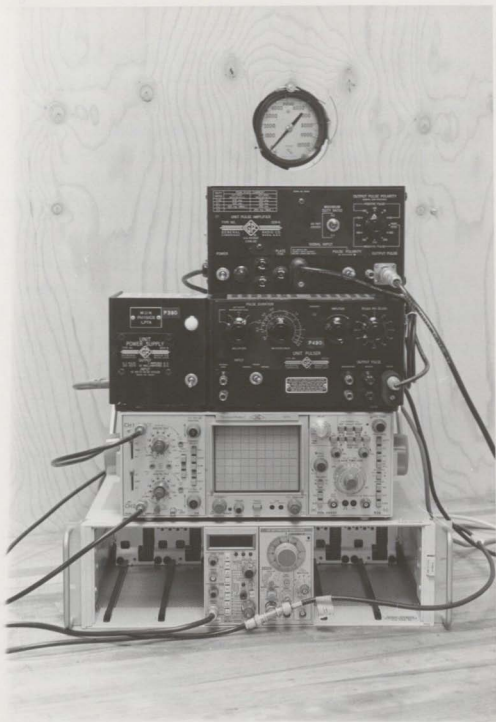


Figure 4. Block diagram of the complete system used for velocity determinations.

Figure 5. Photograph of pressure gauge, pulse generator, dual trace oscilloscope, function generator, and universal counter arranged from top to bottom.



devices and technique just described made it unnecessary to use a mercury delay line.

(b) Acoustic coupling and offset determination

One of the problems encountered when setting up the apparatus was that of establishing and maintaining good and uniform coupling between the sample and the transducers. During initial experiments thin soft solder discs ($\approx .05$ mm thick) were used to provide acoustic coupling between the rock faces and endplugs. After a few complete pressure cycles I noticed that transit times for decreasing pressures were higher than those for increasing pressure on the same run. This is the opposite of what one expects. It was discovered that as the pressure increased the soft copper bottom of the plugs was pressed against the rock allowing a certain amount of hydraulic oil between transducer and the copper. This amount increased as the pressure increased. For pressures decreasing from maximum, the copper remained against the rock. This meant that the copper transducer coupling was interrupted by less oil during the increasing portion of the pressure cycle than for the decreasing part. By placing a thin piece of strong spring steel (.08 mm) between the copper bottom of the endplug and the soft solder disc, which rested against the rock, the situation was remedied. The steel prevented the copper sheet from being pushed into the end of the rock. Also later it was found that brass sheet (.03 mm) could be softened by the heat of a Bunsen burner so that it could be used instead of

the soft solder discs to provide acoustic coupling. Previous to this the solder discs had to be hammered down from a thicker piece. These solder discs were not generally the same thickness, which meant that a different travel time zero point offset had to be determined for each disc. The uniform thickness of the brass sheets, however, required only one offset determination for all the brass discs used.

In any experiment designed to measure acoustic travel time through a substance, it is also necessary to account for time delays of an electrical and mechanical nature associated with the apparatus itself.

Typically offsets for shear and compressional waves are determined by using a series of cylinders of various length of some material with a well-known velocity, or by simply placing the transducer endplugs together face to face. As a precaution I used both methods and found that to within the limits of accuracy, ± 10 ns, the same offsets were obtained at atmospheric pressure. However, the literature does not refer to possible offset change with pressure. By placing the endplugs together, protected by a jacket, and carrying out a pressure run I did observe a small, but noticeable, change. Since the change might be related to the softness of the thin copper sheets of the endplugs, I tried jacketing two pieces of solid brass, each more than 5 mm in thickness, with just P ceramics at the ends and with no copper sheet. The offset again changed. If the confining

medium is allowed to enter between the brass pieces, (i.e. no jacket used), there is no change in offset. The same is true for two thin sheets of copper. If they are sealed at the edges with solder so that no oil gets between them, a change of offset is observed, whereas just two sheets, not sealed, exhibit no change of offset. I conclude that the acoustic coupling between the metals alters somewhat with increasing hydrostatic pressure. This probably also happens when a rock is in the system; however, it is difficult to account for it quantitatively since the effect may be more pronounced with some rocks than with others, depending on the nature of the coupling between rock and endplugs. For example an experiment was run on a sediment which gave a particular travel time change for the total pressure range. A smaller piece of the same rock approximately 1/4 the original length exhibited a total travel time change of about 1/4 that of the larger sample. This would not have been the case had there been any significant change of offset. On the other hand a small piece of granite less than 5 mm in length showed a travel time change comparable to the offset change observed with the endplugs face to face.

Bearing this in mind the velocity results stated in this work will assume constant offset, that is, the offset that was observed with the endplugs face to face at the lower side of the hydrostatic pressure range. For P-waves this was $2.470 \pm 0.1 \mu\text{s}$ and for shear waves $4.070 \pm 0.1 \mu\text{s}$. At maximum pressure these offsets reduced to $2.418 \mu\text{s}$ and $3.930 \mu\text{s}$ respectively.

The experimental arrangement is such that travel time changes of 10 ns, which correspond to relative velocity accuracies of at least .1%, can easily be measured. However, the absolute accuracy of P-S-wave velocities is restricted by the variability of offset. The absolute accuracy for the P and S-wave velocities is obtained by dividing the degree of offset variability by minimum travel times for P and S-waves. For P-waves this is

$$(2.47 - 2.42)\mu\text{s} / 5\mu\text{s} \times 100\% = 1\%$$

and for S-waves,

$$(4.07 - 3.93)\mu\text{s} / 9\mu\text{s} \times 100\% = 1.6\%$$

Therefore, I am claiming 1% accuracy for P-waves and 2% for S-waves, bearing in mind possible polarization effects for S-waves which shall be discussed later (Page 57).

An important feature of this apparatus is the ability to determine P and S-wave velocities on a particular sample with only one pressure cycle. This is advantageous because hysteresis effects can be quite pronounced for rocks, especially porous sediments; and it is, therefore, desirable to obtain concurrent P and S-wave travel times which correspond to the same points in the stress-temperature-history of a given rock. Also, stacking the ceramic transducers enables a complete experiment to take approximately half the time necessary to obtain similar data using P and S-wave transducers sequentially.

(c) Heating jacket

Though the main emphasis of this work was not the study of the effects of temperature variation on velocities, a heating jacket was constructed and experiments were carried out at a few temperatures in the range 7°C - 90°C . This range is limited by the heating medium, water in this case. Future experiments will probably use oil and therefore be capable of studies at higher temperatures.

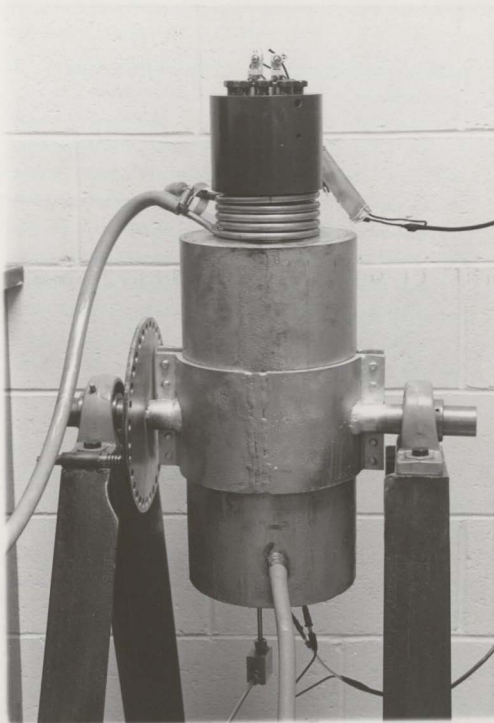
The steel cylindrical jacket is built to fit around the pressure vessel, sealed at the ends with O-rings. A thermostatically controlled bath was used to heat or cool the water and to maintain the temperature in the vessel (Figures 1,4,6).

The temperatures at which experiments were carried out and also small changes ($\approx 3^{\circ}\text{C}$) due to adiabatic heating during pressurization were monitored by a small bead thermistor which was held against the rock samples on the outside of the protective flexible jacket. Due to its high resistance ($\approx 1000\Omega$) it could be connected to ground and the inner brass cylinder on the receiving transducer holder without shunting the signal which goes to the oscilloscope. A digital meter was used to measure its resistance.

In the discussion of results, because of the adiabatic temperature change, graphs illustrating velocity-pressure curves for experiments carried out at slightly different temperatures will be assigned one temperature.



Figure 6. Photograph of the heating jacket
which surrounds the pressure vessel.



2. Preparation and jacketing of samples and measurement procedure

Rock samples are cut into cylinders 23.2 mm in diameter and ranging in length from 25.0 mm to 40.0 mm. End faces are not perfectly parallel, so eight regular spaced measurements of the length are made at the faces and the average is taken to give the effective length for velocity determinations. No corrections are made for contraction during pressurization. Early experiments on saturation using vacuum flooding established that the samples can be saturated by soaking in water at one atmosphere for 24 hours. An air comparison pycnometer was used to measure the effective pore volume allowing the wet density to be calculated from the pore volume and the dry density. A given sample, with spring steel and brass thin discs in place at each end and also the transducer holders in place would have two sleeves of heat shrinkable flexible material in place ready to be shrunk (Figure 1, 2). Silicone glue is applied to the endplugs around the O-ring grooves. When heat is applied, a close fitting flexible jacket forms around the assembly. Two sleeves are used instead of one to insure that no oil leaks into the sample through holes that could possibly develop in the inside jacket if it gets pushed into small cracks and chipped spots on the rock face. After shrinking of both sleeves has taken place, O-rings are pushed on over the jacket and rest in the grooves in the transducer holders. Hydrostatic pressure provides a good seal between jacket and endplugs. When there is no pressure on the sample the silicone glue and the force exerted on the O-rings prevent oil

from leaking into the rock.

An experiment is carried out by first allowing the pressure vessel to stabilize to the desired temperature. Then the pressure is raised in steps and travel times for P and S-waves are recorded at selected pressure values. The same routine is repeated for decreasing pressure. A complete run takes approximately one hour.

The accuracy of the system was tested at atmospheric pressure by using cylinders of copper and fused quartz for which P and S-wave velocities are well documented. The results are tabulated as follows:

Material	Vp (m/s)	Vs* (m/s)
Quartz (Fused)	Handbook* 5968	3764
	Experimental 5962	3746
Copper (Annealed)	Handbook* 4760	2325
	Experimental 4793	2336

*Handbook of Chemistry and Physics (1969-1970)

The experimental velocity values shown in this table agree to well within 1% of the Handbook values.

CHAPTER IV

1. Results and discussion

The core samples used in these experiments came from three Eastern Canadian bore-hole sites (Figure 7): Cormorant N-83 and Coot K-56 on the Grand Banks of Newfoundland and Herjolf M-92 on the Labrador Shelf. Pairs of Cormorant N-83 cores were taken from each of two depths; one vertical (I) core perpendicular to the plane of the bedding and one transverse (II) core parallel to the bedding plane making up each pair. An additional vertical core was used from a third depth. We refer to these cores as Cormorant N-83 6ofB (I), Cormorant N-83 6ofB (II), Cormorant N-83 7ofB (I), and Cormorant N-83 8ofB (I), Cormorant N-83 8ofB (II). The designation 6ofB means that the sample comes from the 6th of 8 evenly spaced sampling levels, each roughly 1.2 m deeper than the previous, beginning at 2360.4 m. Hence Cormorant N-83 6ofB samples come from 2367.7 m, Cormorant N-83 7ofB from 2368.9 m, and Cormorant N-83 8ofB from 2369.8 m. For the Herjolf M-92 bore-hole only vertical cores were available of which two were used, one from a depth of 2636.5 m, Herjolf M-92#14, and one from 2637.1 m, Herjolf M-92#15. One other vertical core used came from the Coot K-56 bore-hole at a depth of 3262.3 m, Coot K-56 4of5 (I). For descriptions, properties and locations of all samples see Table 2.

Figure 7. Map showing well sites on the Grand Banks of Newfoundland and the Labrador Shelf.

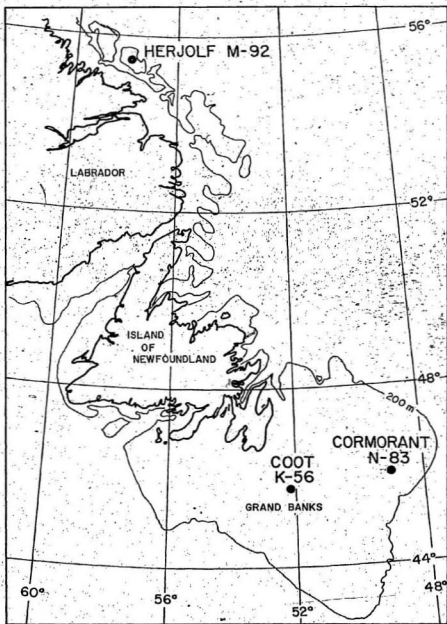


TABLE 2
Locations, properties and descriptions of core samples

SAMPLE	WELL LOCATION		AGE	DRY DENSITY (g/cm ³)	SATURATED DENSITY (g/cm ³)	EFFECTIVE POROSITY		DEPTH (M)	DESCRIPTION AND COMPOSITION
	┆					┆			
CORMORANT N-83, 6 of 8	LATITUDE 46°02'45"N		LOWER JURASSIC	2.931	2.939	┆	.83%	2367.7	Unevenly distributed Dolomite and Anhydrite
	LONGITUDE 48°58'02"W			2.927	2.932		.49%		
CORMORANT N-83, 7 of 8 (1)	LATITUDE 45°45'42"N		LOWER JURASSIC	2.677	2.716	┆	3.90%	2368.9	Dolomite and nodular Anhydrite
	LONGITUDE 52°08'32"W			2.906	2.928		1.25%		
COOT N-56 4 of 5 (A)	LATITUDE 55°31'53"N		LOWER CRETACEOUS	2.904	2.920	┆	1.53%	2369.8	Interbedded Dolomite and Anhydrite
	LONGITUDE 57°04'43"W			2.763	2.780		1.74%		
HERJOLF N-92 #14 (1)	LATITUDE 55°31'53"N		LOWER CRETACEOUS	2.152	2.362	┆	17%	2636.5	Fine grained thinly laminated quartz sandstone. Less than 5% Feldspar and opaques
	LONGITUDE 57°04'43"W			2.218	2.388		17%		
HERJOLF N-92 #15 (1)	LATITUDE 55°31'53"N		LOWER CRETACEOUS	2.218	2.388	┆	17%	2637.1	Fine to medium grained cross laminated quartz sandstone. Between 5% and 10% opaques.

The series of graphs representing the data from Tables 3, 4, 5, 6, 7 is intended to facilitate easy comparison of transverse and vertical cores of the same rock, and also to show the effect of saturation. It should be noted here that when comparisons of the different states of the same or differing samples are made, that is different temperatures or dry and saturated conditions, I will be referring to the portion of the curves which represents descending pressure. In this manner we minimize temperature and pressure history differences between each run. This is evident from the high degree of similarity in shape of the descending portion of curves whereas the ascending pressure curves differ considerably with each experiment. For example see Figures 8, 9 of Coot K-56 4of5 (L).

All tabulated data were obtained using thin brass discs as acoustic coupling between samples and the transducer holders except for Cormorant N-83 7of8 (L). In this case soft solder discs were used. This sample suffered considerable damage on a subsequent saturation before I started using brass discs.

(a) Anisotropy and hysteresis

One factor common to all data was that of hysteresis. While not so great for sample Cormorant N-83 8of8 (II), (Figures 10, 11) it was quite evident in other samples and especially pronounced for Coot K-56 4of5 (L) and Cormorant N-83 7of8 (L) (Figures 8, 9, 12). Significant hysteresis was also noted for the Herjolf M-92 samples though complete ascending and descending pressure data was

TABLE 3
 Compressional and shear wave velocities of Cormorant N-83 80f8
 samples throughout complete pressure cycles

Pressure	V_p (km/s)	V_s (km/s)						
6.895 MPa	5.479	2.643	5.318	2.575	5.132	2.473	5.142	2.552
	5.555	2.668	5.411	2.602	5.145	2.495	5.148	2.537
	5.681	2.785	5.579	2.650	5.164	2.552	5.164	2.583
	5.763	2.731	5.688	2.685	5.181	2.609	5.181	2.577
	5.817	2.750	5.741	2.700	5.218	2.685	5.218	2.591
	5.874	2.763	5.814	2.716	5.231	2.670	5.231	2.603
	5.903	2.775	5.859	2.732	5.239	2.675	5.239	2.617
	5.942	2.783	5.893	2.742	5.247	2.678	5.247	2.630
	5.978	2.789	5.927	2.748	5.260	2.683	5.260	2.644
	5.955	2.789	5.905	2.747	5.254	2.679	5.254	2.642
	5.913	2.785	5.872	2.739	5.243	2.676	5.243	2.641
	5.888	2.775	5.844	2.731	5.236	2.671	5.236	2.634
	5.843	2.764	5.795	2.720	5.224	2.667	5.224	2.627
	5.794	2.746	5.735	2.702	5.201	2.660	5.201	2.613
	5.718	2.718	5.666	2.681	5.189	2.656	5.189	2.598
	5.584	2.678	5.526	2.643	5.165	2.651	5.165	2.578
	5.486	2.648	5.412	2.620	5.148	2.646	5.148	2.552

CORMORANT N-83, 80f8 (I) CORMORANT N-83, 80f8 (II) CORMORANT N-83, 80f8 (L) CORMORANT N-83, 80f8 (L)
 DRY DRY DRY DRY
 V_p (km/s) V_p (km/s) V_p (km/s) V_p (km/s)
 V_s (km/s) V_s (km/s) V_s (km/s) V_s (km/s)
 29°C 29°C 26°C 26°C

Compressional and shear wave velocities for Cormorant N-83 607d and
Cormorant N-83 607b samples throughout complete pressure cycles

TABLE 4

PRESSURE x 6.895 MPa	CORMORANT 8 of 8 (11) H ₂ O SATURATED 70c		CORMORANT 8 of 8 (11) H ₂ O SATURATED 210c		CORMORANT 6 of 8 (T) DRY 80c		CORMORANT 6 of 8 (11) DRY 80c	
	V_p (km/s)	V_s (km/s)	V_p (km/s)	V_s (km/s)	V_p (km/s)	V_s (km/s)	V_p (km/s)	V_s (km/s)
0.5	6.138	2.723	6.053	2.705	6.143	2.727	5.971	2.677
1.1	6.147	2.725	6.078	2.707	6.178	2.764	6.036	2.709
2.1	6.152	2.726	6.110	2.712	6.242	2.804	6.106	2.737
3.1	6.163	2.730	6.125	2.715	6.297	2.827	6.159	2.755
4.1	6.192	2.736	6.143	2.716	6.335	2.842	6.215	2.770
5.1	6.199	2.739	6.158	2.718	6.367	2.851	6.261	2.777
6.1	6.212	2.741	6.175	2.719	6.397	2.856	6.299	2.786
7.1	6.230	2.742	6.209	2.719	6.415	2.860	6.325	2.792
8.1	6.231	2.742	6.212	2.727	6.438	2.862	6.347	2.796
7.1	6.229	2.742	6.210	2.723	6.421	2.861	6.332	2.793
6.1	6.212	2.741	6.192	2.721	6.397	2.859	6.302	2.791
5.1	6.209	2.738	6.173	2.719	6.383	2.858	6.280	2.784
4.1	6.196	2.738	6.155	2.718	6.349	2.852	6.246	2.777
3.1	6.180	2.735	6.121	2.717	6.315	2.839	6.206	2.764
2.1	6.158	2.731	6.105	2.712	6.262	2.815	6.146	2.749
1.1	6.151	2.727	6.088	2.709	6.194	2.773	6.058	2.717
0.5	6.139	2.725	6.077	2.706	6.154	2.727	5.998	2.688

Compressional and shear wave velocities for Cormorant N-83 60f8 samples throughout complete pressure cycles

PRESSURE x 6.895 MPa	CORMORANT N-83 60f8 (L) H ₂ O SATURATED 90°C		CORMORANT N-83, 60f8(II) H ₂ O SATURATED 90°C		CORMORANT N-83, 60f8(L) H ₂ O SATURATED 740°C		CORMORANT N-83, 60f8(T) H ₂ O SATURATED 480°C	
	V _p (km/s)	V _s (km/s)	V _p (km/s)	V _s (km/s)	V _p (km/s)	V _s (km/s)	V _p (km/s)	V _s (km/s)
8.5	6.183	2.715	6.213	2.659	—	2.709	6.098	2.598
1.1	6.214	2.749	6.247	2.698	—	2.723	6.106	2.719
2.1	6.308	2.788	6.296	2.728	—	2.758	6.240	2.747
3.1	6.326	2.797	6.340	2.743	—	2.768	6.257	2.758
4.1	6.374	2.800	6.358	2.755	—	2.772	6.315	2.763
5.1	6.412	2.802	6.382	2.761	—	2.782	6.338	2.770
6.1	6.421	2.802	6.400	2.765	—	2.786	6.358	2.770
7.1	6.431	2.804	6.417	2.767	—	2.788	6.375	2.772
8.1	6.439	2.804	6.437	2.769	—	2.790	6.384	2.775
7.1	6.431	2.803	6.413	2.761	—	2.785	6.361	2.772
6.1	6.397	2.801	6.389	2.757	—	2.776	6.345	2.766
5.1	6.379	2.799	6.365	2.748	—	2.769	6.288	2.762
4.1	6.371	2.798	6.340	2.742	—	2.765	6.279	2.759
3.1	6.320	2.792	6.319	2.729	—	2.753	6.233	2.753
2.1	6.240	2.773	6.273	2.710	—	2.725	6.183	2.733
1.1	6.184	2.745	6.217	2.679	—	2.691	6.130	2.719
0.5	6.131	2.714	6.203	2.650	—	2.657	6.075	2.686

TABLE 5

TABLE 6

Compressional and shear wave velocities for Coot K-56 4off- (L) and compressional velocities for Coromant N-83 7off8 (L) throughout complete pressure cycles

PRESSURE x 6.895 Mbar	COOT k-56, 4 of 5 (L) DRY 90°C		COOT k-56, 4 of 5 (L) DRY 230°C		COOT k-56, 4 of 5 (L) H ₂ O SATURATED 260°C		COROMANT N-83, 7off8 (L) DRY 210°C	
	V _p (km/s)	V _s (km/s)	V _p (km/s)	V _s (km/s)	V _p (km/s)	V _s (km/s)	V _p (km/s)	V _s (km/s)
0.6	6.230	2.720	5.874	2.627	5.577	5.366	3.612	—
1.1	6.325	2.745	6.027	2.654	6.641	6.468	3.718	—
2.1	6.395	2.779	6.181	2.704	6.711	6.529	3.888	—
3.1	6.459	2.805	6.298	2.742	6.775	6.620	4.021	—
4.1	6.525	2.826	6.375	2.772	6.828	6.687	4.154	—
5.1	6.581	2.848	6.471	2.798	6.863	6.792	4.257	—
6.1	6.640	2.862	6.554	2.820	6.896	6.880	4.361	—
7.1	6.692	2.873	6.623	2.839	6.928	6.899	4.443	—
8.1	6.761	2.884	6.692	2.855	6.962	6.934	4.515	—
7.1	6.725	2.879	6.675	2.848	6.929	6.901	4.478	—
6.1	6.694	2.875	6.638	2.844	6.912	6.883	4.487	—
5.1	6.654	2.865	6.588	2.830	6.888	6.844	4.337	—
4.1	6.601	2.847	6.550	2.816	6.865	6.810	4.243	—
3.1	6.548	2.830	6.496	2.797	6.829	6.773	4.140	—
2.1	6.480	2.803	6.414	2.775	6.780	6.669	4.007	—
1.1	6.346	2.761	6.305	2.734	6.691	6.565	3.818	—
0.6	6.279	2.733	6.213	2.656	6.620	6.497	3.678	—

TABLE 4
Compressional and shear wave velocities for HerJolf M-92
samples taken along a geotherm

GEOTHERM DEPTH (m)	HERJOLF M-92 # 14 DRY		HERJOLF M-92 # 15 DRY		HERJOLF M-92 # 14 H ₂ O SATURATED		HERJOLF M-92 # 15 H ₂ O SATURATED	
	V_p (cm/s)	V_s (cm/s)	V_p (cm/s)	V_s (cm/s)	V_p (cm/s)	V_s (cm/s)	V_p (cm/s)	V_s (cm/s)
	500	2.204	1.753	2.469	1.926	3.037	1.822	2.967
1000	2.501	1.951	2.671	2.033	3.254	1.971	3.205	1.526
1500	2.773	2.114	2.909	2.167	3.393	2.082	3.350	1.585
2000	2.989	2.238*	3.104	2.269	3.527	2.173	3.468	1.634
2500	3.213	2.362*	3.321	2.383*	3.666	2.216	3.603	1.690
3000	3.388	2.453*	3.546	2.495*	3.784	2.263	3.692	1.722

*These velocities are extrapolated because the shear wave became distorted.

P-WAVE VELOCITIES

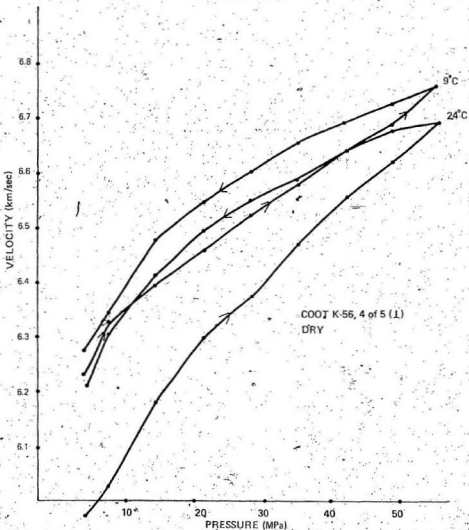


Figure 8. Compressional wave velocity as a function of hydrostatic pressure for Coot K-56 4 of 5 (L) at two temperatures in the dry state. The relative error in velocity is comparable to the size of the dots on this and subsequent graphs.

S-WAVE VELOCITIES

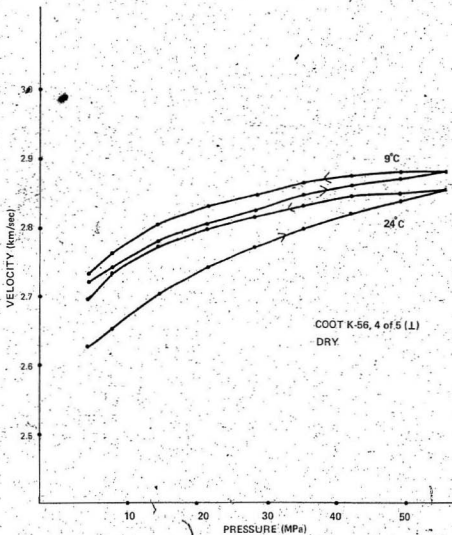


Figure 9. Shear wave velocity for Coot K-56 4of5 (L) as a function of hydrostatic pressure at two temperatures in the dry state.

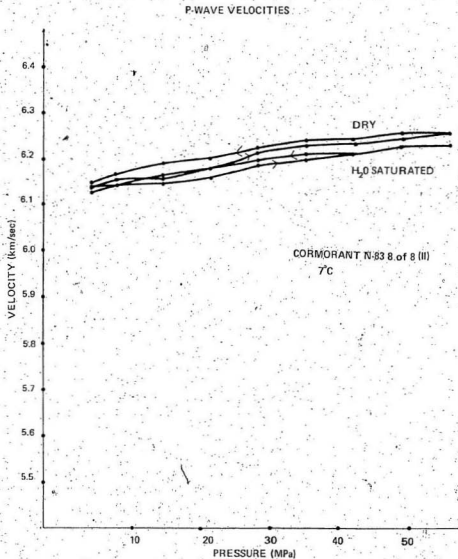


Figure 10. Compressional wave velocity for Cormorant N-83 8 of 8 (II) as a function of hydrostatic pressure in dry and water saturated states.

S-WAVE VELOCITIES

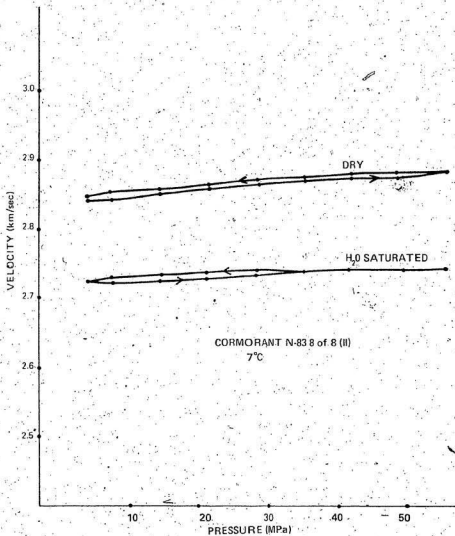


Figure 11. Shear wave velocity as a function of hydrostatic pressure for Cormorant N-83 8 of 8 (II) in dry and water saturated states.

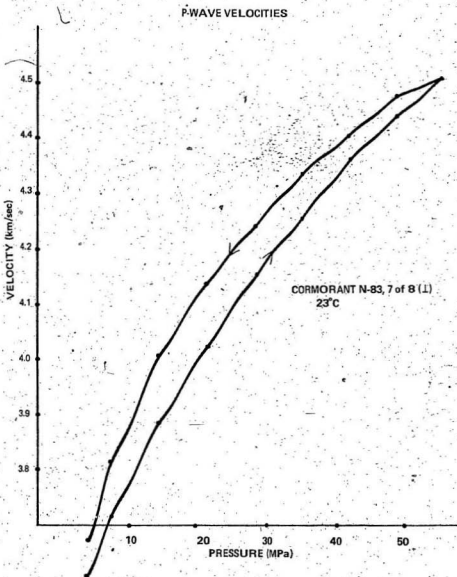


Figure 12. Compressional wave velocity as a function of hydrostatic pressure for Cormorant N-83 7 of 8 (L) in the dry state.

not obtained due to the different nature of the experiments carried out on those two particular cores.

With the Cormorant N-83 8of8 series (Figures 13, 14, 15, 16) hysteresis is more evident in the sample perpendicular to the bedding than in the transverse one. Also velocities are higher in the transverse sample than in the vertical sample. On the other hand the Cormorant N-83 6of8 series (Figures 17, 18, 19, 20) higher velocities occur in the vertical sample and hysteresis is approximately the same for the vertical and transverse cores. This situation merits some discussion.

There are at least three possible causes of velocity anisotropy: 1. Alignment, in the plane of the bedding, of pores and cracks, 2. the preferred orientation of anisotropic crystals such as calcite, for which Dandekar (1968) found compressional wave velocity along the crystallographic c-axis to be 5.61 km/s, and in a direction normal to the c-axis 7.35 km/s, and 3. inhomogeneous distribution of rock constituents and preferred orientation of such inhomogeneities. Mechanical and/or chemical processes could be responsible for these conditions. It is also conceivable that two or more of these versions of anisotropy could coexist in a given sample. From my data I conclude that the dominant anisotropic mechanism for the Cormorant N-83 8of8 samples is alignment of cracks and pores, and for the Cormorant N-83 6of8 samples the mechanism is the inhomogeneous distribution and orientation of the rock constituents. These deductions are supported as follows. Pores and cracks tend to close under increasing pressure. Because of crack alignment horizontal

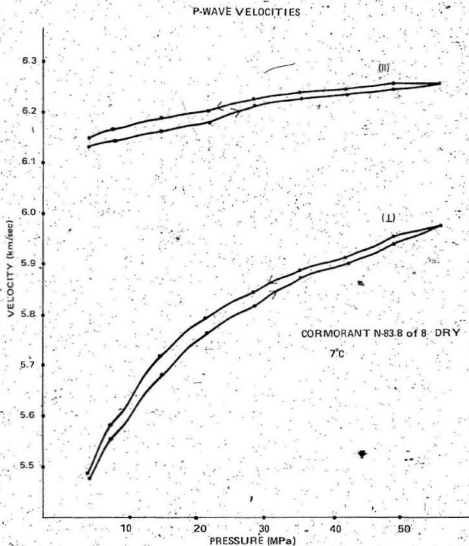


Figure 13. Compressional wave velocity as a function of hydrostatic pressure for vertical and transverse Cormorant N-83 Bof8 samples in the dry state.

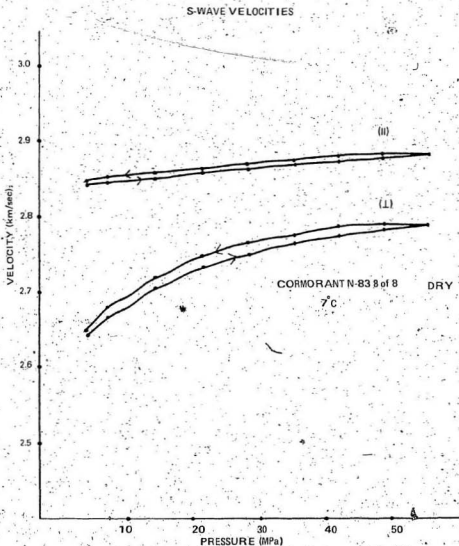


Figure 14. Shear wave velocity as a function of hydrostatic pressure for vertical and transverse Cormorant N-83 8 of 8 samples in the dry state.

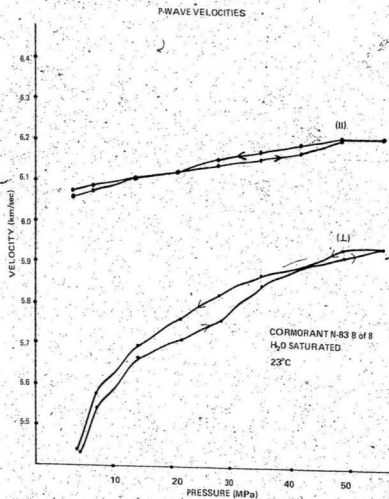


Figure 15. Compressional wave velocity as a function of hydrostatic pressure for water saturated vertical and transverse Cormorant N-83 8 of 8 samples.

S-WAVE VELOCITIES

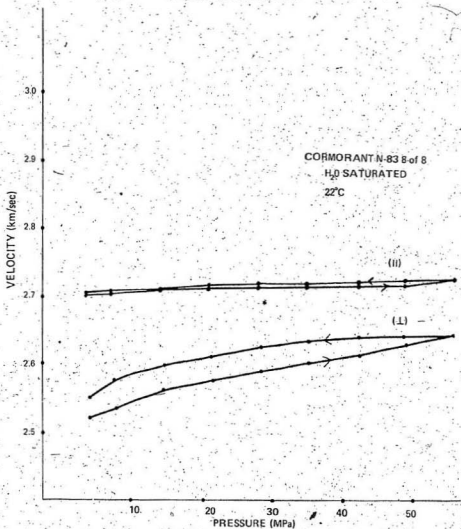


Figure 16. Shear wave velocity as a function of hydrostatic pressure for water saturated vertical and transverse Cormorant N-83 Bof8 samples.

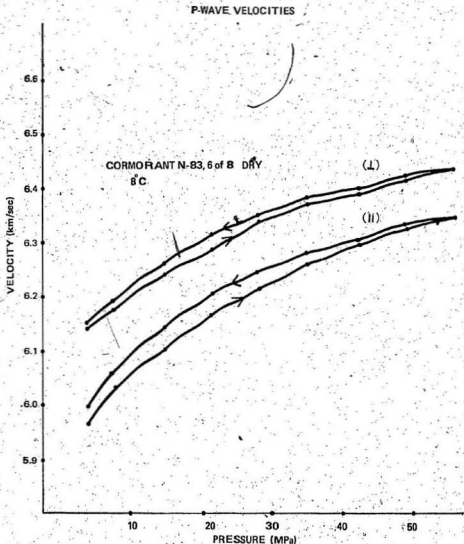


Figure 17. Compressional wave velocity as a function of hydrostatic pressure for vertical and transverse Cormorant N-83 6of8 samples in the dry state.

S-WAVE VELOCITIES

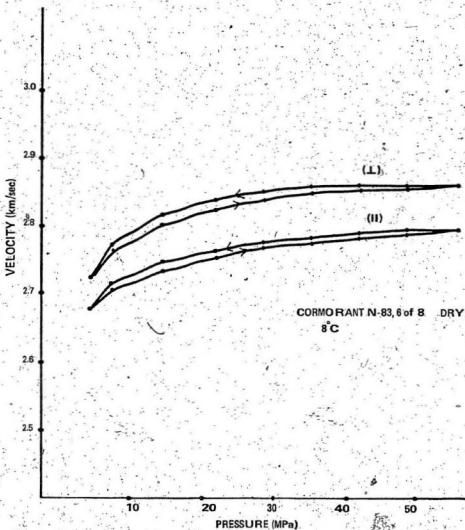


Figure 18. Shear wave velocity as a function of hydrostatic pressure for vertical and transverse Cormorant N-83 6 of 8 samples in the dry state.

P-WAVE VELOCITIES

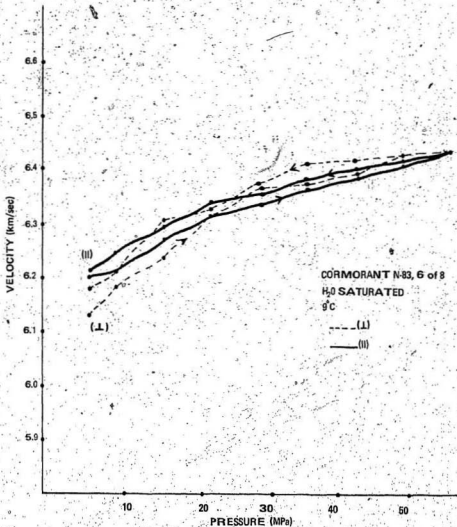


Figure 19. Compressional wave velocity as a function of hydrostatic pressure for vertical and transverse Cormorant N-83 6of8 samples in the water saturated state.

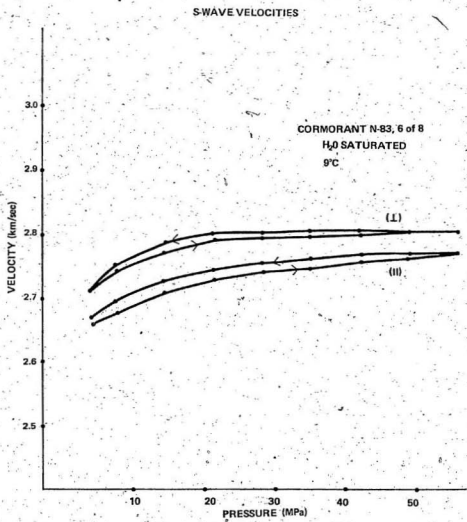


Figure 20. Shear wave velocity as a function of hydrostatic pressure for vertical and transverse Cormorant N-83 6 of 8 samples in the water saturated state.

to the bedding there is less opening and closing in the transverse sample, and hence less hysteresis. (Schreiber et al. (1972), Christensen et al. (1973)). Velocity of shear and compressional waves would be higher in the transverse sample where there is more grain boundary contact in the direction of wave propagation than in the vertical sample. The degree of anisotropy would, however, be expected to decrease with increasing pressure since pores and cracks would then close. The effects just described are precisely what was observed in the Cormorant N-83 8of8 samples (Figures 13, 14, 15, 16).

In the case of the third type of anisotropy, we would expect the difference in velocities of transverse and vertical cores to remain fairly constant with changes in hydrostatic pressure. In the same vein if there is no preferred alignment of cracks and pores, vertical and transverse samples would exhibit similar degrees of hysteresis. Furthermore, either sample could show the higher velocity depending on the distribution and orientation of the rock constituents. Figures 17, 18, 19, 20 demonstrate similar degrees of hysteresis in transverse and vertical samples and also a higher velocity exhibited in the vertical core. These samples consist of anhydrite and dolomite in visibly uneven distribution. No calcite is present. All of these facts are strongly consistent with the third type of anisotropy.

(b) Note on polarization effects

When Cormorant N-83 6of8 (II) was put between the end-plugs with bedding lines perpendicular to the transverse motion of the shear wave crystal, easily distinguishable shear wave signals were obtained. Rotating the rock 90° relative to the endplugs resulted in a very poor shear wave signal, making it virtually impossible to see the first negative shear wave peak. Rotating back to the original configuration resulted in a good signal again. The same test on the Cormorant N-83 8of8 (II) sample showed the quality of the shear wave signal not to be as greatly affected by polarization as was Cormorant N-83 6of8 (II), however, the travel time appeared to change slightly, $\approx .1\mu s$. This travel time change may be the result of polarization. I conclude from these observations that shear wave quality may be a significant function of polarization for certain transverse core samples and that S-wave velocity may also be affected slightly by polarization.

(c) Effects of saturation

According to Biot's Theory, saturation of porous rocks would tend to increase compressional wave velocities and decrease shear wave velocity. For shear waves this has been verified for the Cormorant N-83 6of8 samples, Cormorant N-83 8of8 samples, and Herjolf M-92#15 at all pressures (Figures 11, 21, 22, 23, 24) and for Herjolf M-92#14 at pressures above ≈ 15 MPa (Figure 25). King (1966) had observed a similar crossover behaviour for St. Peter Sandstone, as I noted for Herjolf M-92#14. For moderately low pressures the interaction of saturant and detrital material is

S-WAVE VELOCITIES

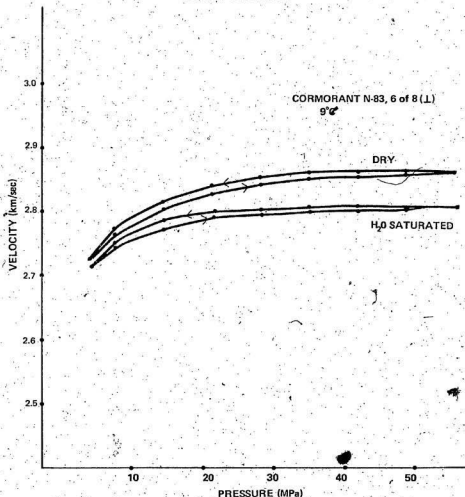


Figure 21. Shear wave velocity as a function of hydrostatic pressure for Cormorant N-83 6 of 8 (L) in dry and water saturated states.

S-WAVE VELOCITIES

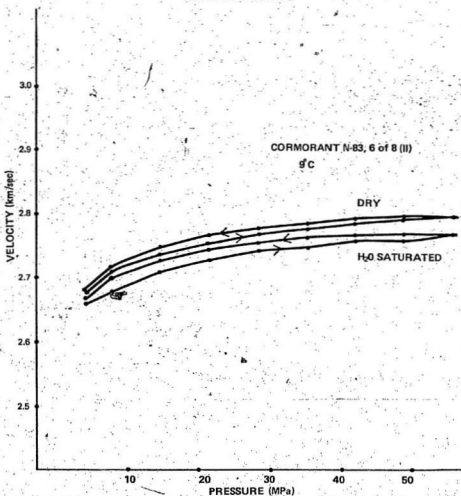


Figure 22. Shear wave velocity as a function of hydrostatic pressure for Cormorant N-83 6of8 (II) in dry and water saturated states.

S WAVE VELOCITIES

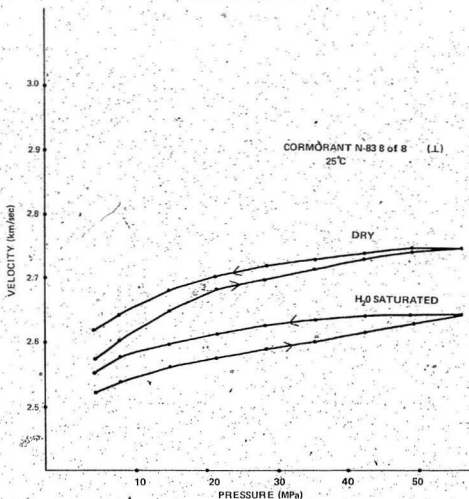


Figure 23. Shear wave velocity as a function of hydrostatic pressure for Cormorant N-83 8 of 8 (L) in dry and water saturated states.

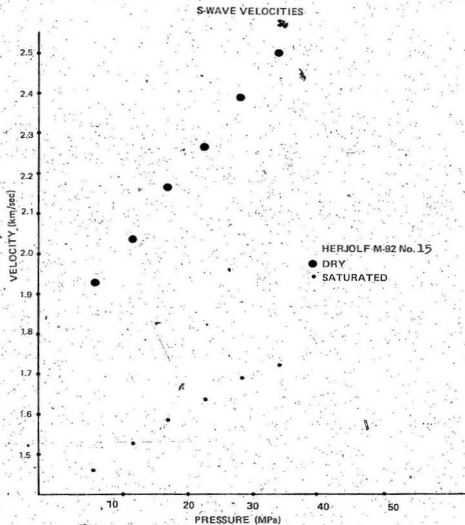


Figure 24. Shear wave velocity as a function of position along a geotherm for Herjolf M-92#15 in dry and water saturated states.

S-WAVE VELOCITIES

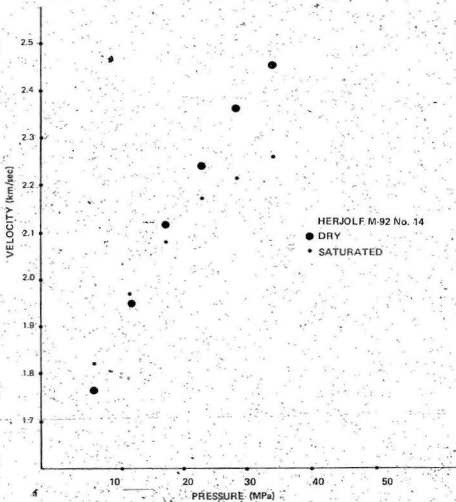


Figure 25. Shear wave velocity as a function of position along a geotherm for Herjolf M-92#14 in dry and water saturated states.

thought to influence significantly ultrasonic velocities in sandstone. The effects of relaxation behaviour of the saturant in cracks and pores, and also the influence of liquids on interfacial surface phenomena affect velocities. I think that increasing the pressure, above 15 MPa in my case, reduces these interactions by crack and pore closure and the velocities approach those predicted by Biot. Compressional wave velocities are affected by saturation in a way which agrees qualitatively with Biot's predicted increase for all our samples (Figures 26 to 31) except Cormorant N-83 8of8 (II) (Figure 10). I suspect that saturation weakens the solid matrix structure and grain boundary contacts. The transverse Cormorant N-83 8of8 sample, which undergoes little change in the total number of "effective" contacts in the direction of wave propagation with saturation, would then show a decrease in V_p due to contact and structure weakening whereas the vertical Cormorant N-83 8of8 (Figure 17) sample would experience a significant increase in "effective" grain boundary contacts when fluid fills pores and cracks that lie in a direction perpendicular to the P-wave direction. The "effective" increase in grain boundary contacts due to the saturant has a greater influence than the weakening of solid matrix contacts and structure. Hence compressional wave velocity increases with saturation for the vertical sample.

2

P-WAVE VELOCITIES

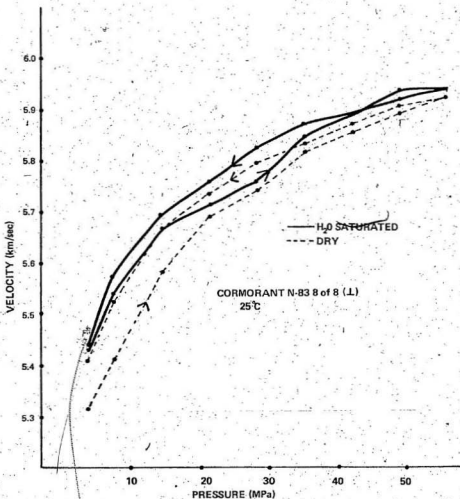


Figure 26. Compressional wave velocity as a function of hydrostatic pressure for Cormorant N-83 BofB (L) in dry and water saturated states.

P-WAVE VELOCITIES

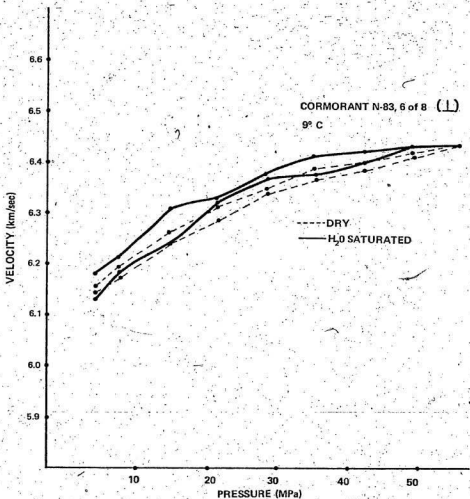


Figure 27. Compressional wave velocity as a function of hydrostatic pressure for Cormorant N-83 6of8 (L) in dry and water saturated states.

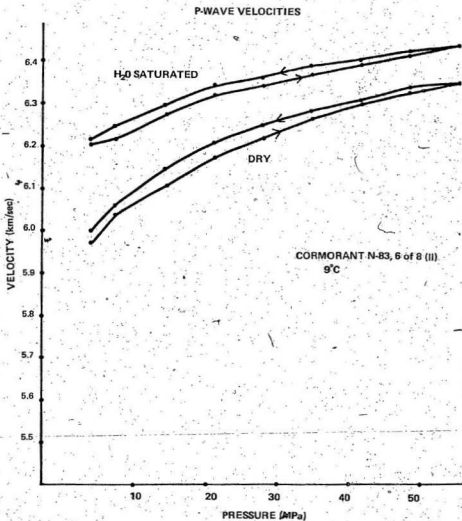


Figure 28. Compressional wave velocity as a function of hydrostatic pressure for Cormorant N-83 6of8 (II) in dry and water saturated states.

P-WAVE VELOCITIES

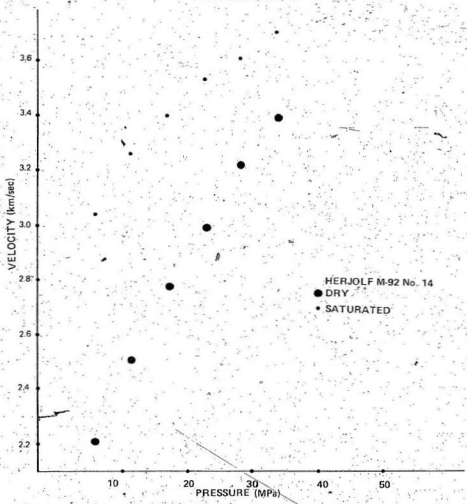


Figure 29. Compressional wave velocity as a function of position along a geotherm for Herjolf M-92#14 in dry and saturated states.

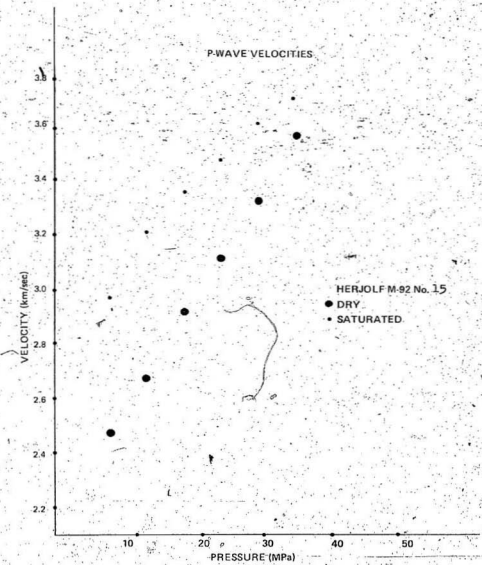


Figure 30. Compressional wave velocity as a function of position along a geotherm for Herjolf M-92#15 in dry and saturated states.

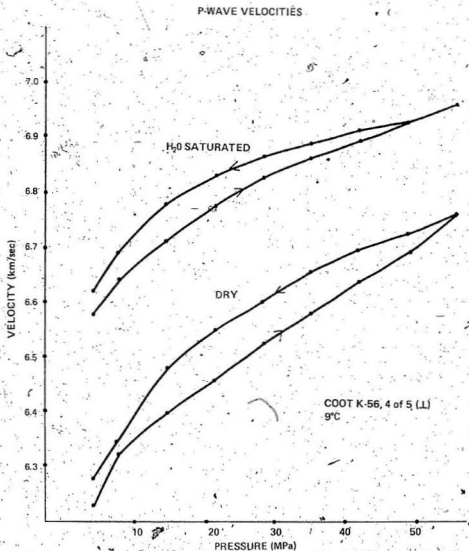


Figure 31. Compressional wave velocity as a function of hydrostatic pressure for Coot K-56 4 of 5 (L) in dry and water saturated states.

(d) Comparison with in situ well logs

Results were compared with the acoustic logs where possible. Where the part of the log corresponding to the sample's depth exhibits no great fluctuations in travel times over at least a 2m section, my results invariably showed the laboratory measurements of velocity to be greater than the well log velocities (Table 8). Jones and Wang (1981) obtained qualitatively similar results for Cretaceous Shales. They cite bias in sampling, dispersion due to different frequencies used with laboratory and logging devices, formation damage during drilling, and differences in scale of laboratory and bore-hole measurements as possible reasons to explain, at least partially, the observed discrepancy. In general it is difficult to say which has the greatest effect, since the condition and lithology of different bore-holes and different sections of the same bore-hole vary greatly. However, Jones and Wang (1981) do calculate a possible 4% reduction in bore-hole measurements due to dispersion. This is not adequate to explain the discrepancies (10%) which they observed. For my results even an exaggerated 10% reduction due to dispersion could not account for the discrepancies (22% - 36%) observed. Not having access to a well logging device or the procedure for its calibration and use, I find it hard to comment any further, though I would suggest one other possibility, that is, the acoustic coupling between the logging device in a well and the rock wall may not be as good or as uniform as coupling in laboratory experiments. This could introduce a systematic reduction in velocities for well log measurements even though the arrangement of the transducers in the sonde is designed to minimize this problem.

TABLE 8

Comparison of well log compressional
velocities with those obtained in the laboratory

SAMPLE	WELL LOG V_p (km/s) $\pm 5\%$	LABORATORY V_p (km/s) $\pm 2\%$		DISCREPANCY FOR SATURATED CASE
		DRY	SATURATED	
CORMORANT N-83 8 of 8 (1)	4.52	5.75	5.77	22%
COOT K-56 4 of 5 (1)	4.35	6.52	6.85	36%
HERJOLF M-92 # 14	2.77	3.33	3.67	24%
HERJOLF M-92 # 15	2.85	3.48	3.66	22%

(e) Temperature effects

As already stated, the emphasis of this work was not to determine accurately the effects of temperature on seismic velocities. Qualitatively speaking I found that the effects were greater towards the lower end of the available (7°C - 90°C) temperature range. Figures 8, 9 show velocity curves representing two temperatures for Coot K-56 4of5 (L) and Figures 32, 33 show curves for Cormorant N-83 6of8 (L) at three temperatures. In particular Figure 33 demonstrates that the velocity change corresponding to a temperature change from 9°C to 24°C ($\approx 1\%$ in velocity) is as great or greater than that for a temperature change from 23°C to 48°C . This was characteristic of all samples for which complete ascending and descending pressure curves were obtained. The data on the Herjolf M-92 samples (Figures 24, 25, 29, 30) are taken along a geotherm. That is, the first velocity point on a graph corresponds to a temperature and pressure at a depth of 500 m, the second point is for a depth of 1000 m, the next 1500 m, and so on down to 3000 m. The temperature and pressure gradients are 29.7 mK/m and 1131.3 kPa/m respectively. Therefore, the greatest depth (3000 m) corresponds to a temperature of $\approx 90^{\circ}\text{C}$ and a pressure of 34.04 MPa . The rock samples, Lower Cretaceous sandstones, typically exhibit low velocities since the constituents are not very well consolidated.

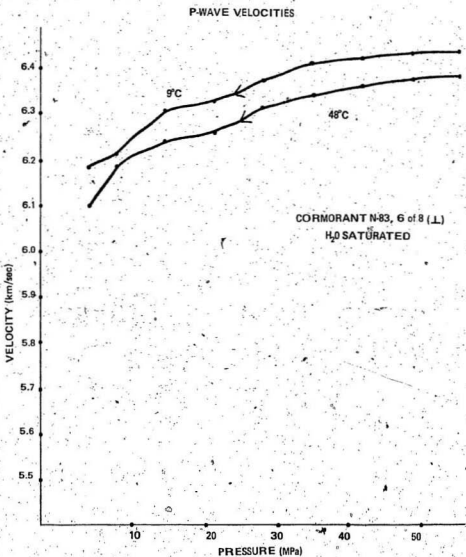


Figure 32. Compressional wave velocity for Cormorant N-83, 6 of 8 (L) at two temperatures in the water saturated state.

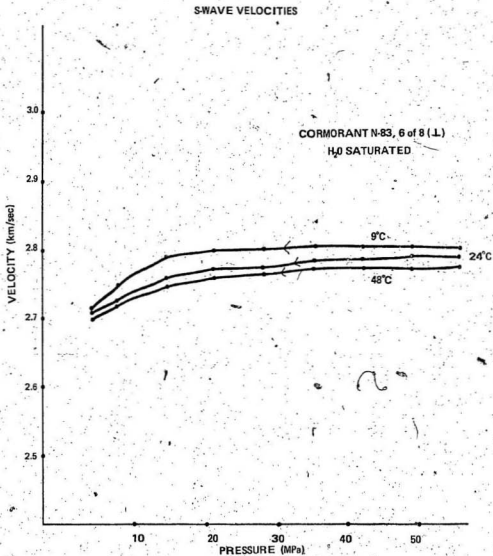


Figure 33. Shear wave velocity as a function of hydrostatic pressure for Cormorant N-83 6of8 (⊥) at three temperatures in the water saturated state.

CHAPTER V

1. Summary

A versatile apparatus has been constructed to determine accurately compressional ($\pm 1\%$) and shear ($\pm 2\%$) wave velocities as functions of temperature and pressure. A new and significant feature of the design, made possible by stacking piezoelectric transmitting and receiving P and S-wave transducers, is the ability to measure both shear and compressional velocities with each experiment. This is particularly important when studying rock samples which have V_p and V_s values that depend to some extent on the rock's stress-temperature history in which case concurrent V_p and V_s are desirable. The instrument has potential for studies of permeability versus pressure and also seismic velocities versus differential pore pressure. Initial experiments on sediments from three different wells on Canada's east coast yielded the following general results.

(1) I found qualitative agreement with Biot's predicted theory of a decrease in shear wave velocity with saturation. This held true for all samples at all pressures except sample Herjolf M-92#14 which required a certain pressure (≈ 15 MPa) before sufficient numbers of cracks and pores had closed to permit agreement with the theory.

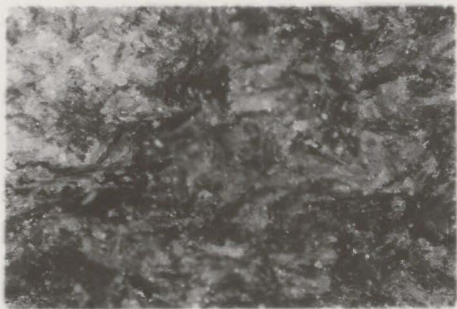
(2) Also there was qualitative agreement with the predicted increase in compressional wave velocity with saturation. This was

true for all cases except Cormorant N-83 8of8 (II) where I conclude that saturation causes weakening of solid matrix structure and grain boundary contacts.

(3) In cases where vertical and transverse cores were available significant degrees of anisotropy were observed (2 - 10%). I propose that for the Cormorant N-83 8of8 samples the dominant mechanism for anisotropy is alignment of cracks and pores in the plane of the bedding and that anisotropy in the Cormorant N-83 6of8 samples is due to inhomogeneous distribution and orientation of rock constituents. To substantiate this, hand and microscopic inspection of the Cormorant N-83 8of8 samples revealed fine veins and homogenized layering of cracks and rock components, anhydrite and dolomite, in the horizontal plane. The Cormorant N-83 6of8 samples, however, show far less homogeneity in the rock constituent intermingling and crack orientation in the plane of the bedding (Figure 34). The former type of anisotropy implies higher elastic wave velocities in the transverse sample, whereas the latter type puts no restriction on which core, the transverse or vertical, should have the higher velocities.

(4) Significant discrepancies were observed between velocities obtained from laboratory and those derived from well logs. Invariably, well log velocities were lower than laboratory P-wave velocities (22% - 36%). Apart from the possible reasons for this quoted by Jones and Wang (1981), I would add further that acoustic coupling may not be as good or as uniform with the well log instrument as with the laboratory apparatus. This systematic error

Figure 34. Side wall views, magnified approximately 100 times, showing fairly homogenized layering of anhydrite and dolomite in the bedding plane in Cormorant N-83 8of8 (Top) and inhomogeneous distribution of anhydrite and dolomite in Cormorant N-83 6of8 (Bottom).



could account in part for lower velocities.

(5) Velocity hysteresis effects were evident in all samples: pronounced in some and minimal in others depending on the quantity and orientation of cracks and pores.

(6) The effect of temperature, which in general is small compared to the influence of hydrostatic pressure, was greatest towards the lower end of the available temperature range (7°C - 90°C).

It was found that a 40°C change in temperature in this range will not affect velocities by more than 2%.

REFERENCES

- Biot, M.A., Generalized Theory of Acoustic Propagation in Porous Dissipative Media, *J. Acoust. Soc. Amer.*, 34 (5), 1254-1264, 1962.
- Birch, F., The velocity of compressional waves in rocks to 10 Kilobars, I, *J. Geophys. Res.*, 65, 1083-1102, 1960.
- Birkhoff, G., *Hydrodynamics*, Copyright ©1960 by Princeton University Press, Printed in the United States.
- Buessem, W.R., Internal ruptures and recombinations in anisotropic ceramic materials, in "Mechanical Properties of Engineering Ceramics," edited by W.W. Krieger and H. Palmour III, Interscience Publishers, New York, 1961.
- Carlson, R. L., and Christensen, N.I., Velocity anisotropy in semi-indurated calcareous deep sea sediments, *J. Geophys. Res.*, 84, B1, 205-211, 1979.
- Christensen, N.I., D.M. Fountain, and R.J. Stewart, Oceanic crustal basement: A comparison of seismic properties of DSDP basalts and consolidated sediments, *Mar. Geol.*, 15, 215-226, 1973.
- Dandekar, D.P., Elastic constants of calcite, *J. Appl. Phys.*, 39, 2971-2973, 1968.
- Desai, K.P., D.P. Helander, and E.J. Moore, Sequential measurement of compressional and shear velocities of rock samples under uniaxial pressure, *Soc. Petrol. Eng. J.*, 9, 378-394, 1969.
- Gardner, G.H.F., Wyllie, M.R.J., and Droschak, D.M., Effects of pressure and fluid saturation on the attenuation of elastic waves in sands: *J. Petrol. Tech.*, 16, 189-198, 1964.
- Hysteresis in velocity-pressure characteristics of rocks: *Geophysics*, 30, 111-116, 1965.
- Hughes, D.S., and Cross, J.H., Elastic wave velocities in rocks at high pressures and temperatures, *Geophysics*, 16, 577-593, 1951.

- Hughes, D. S., and H. J. Jones, Elastic wave velocities in sedimentary rocks. *Eos Trans. AGU*, 32, 173-178, 1951.
- Hughes, D. S., and J. L. Kelly, Variation of elastic wave velocity with saturation in sandstone. *Geophysics*, 17, 739-752, 1952.
- Jones, L. E. A., and H. F. Wang, Ultrasonic velocities in Cretaceous shales from the Williston basin, *Geophysics*, 46 (3), 288-297, 1981.
- King, M. S., Wave velocities in rocks as a function of changes in overburden pressure and pore fluid saturants, *Geophysics*, 31, 50-73, 1966.
- King, M. S., and Fatt, I., Ultrasonic shear-wave velocities in rocks subjected to simulated overburden pressure: *Geophysics*, 27, 590-598, 1962.
- O'Connell, R. J., and B. Budiansky, Seismic velocities in dry and saturated cracked solids, *J. Geophys. Res.*, 79, 5412-5426, 1974.
- Peselnick, L., Elastic constants of Solenhofen limestone and their dependence upon saturation and density: *J. Geophys. Res.*, 67, 4441-4448, 1962.
- Peselnick, L., and Ziétz, I., Internal friction of fine grained limestones at ultrasonic frequencies: *Geophysics*, 24, 285-296, 1959.
- Schreiber, E., J. Fox, and J. Petersen, Compressional sound velocities in semi-indurated sediments and basalts from DSDP Leg 11, in Hollister, D.C., J. I. Ewing et al., Initial Reports of the Deep Sea Drilling Project, 11, edited by C.D. Hollister et al., 723, U.S. Government Printing Office, Washington D.C., 1972.
- Simmons, G., Velocity of shear waves in rocks to 10 Kilobars; Part I: *J. Geophys. Res.*, 69, 1123-1130, 1964.
- Stewart, R. M., and Peselnick, L., Velocity of compressional waves in dry franciscan rocks to 8 kbar and 300°C, *J. Geophys. Res.*, 82, 2027-2039, 1977.
- Toksöz, M. N., Johnston, D. H., and Timur, A., Attenuation of seismic waves in dry and saturated rocks. I. Laboratory measurements: *Geophysics*, 44, 4, 681-690, 1979.

Tolstoy, I., Wave Propagation, Copyright © 1973 by McGraw-Hill, Inc. Printed in the United States.

Wyllie, M.R.J., Gregory, A.R., and Gardner, L.W., Elastic wave velocities in heterogeneous and porous media: *Geophysics*, 21, 41-70, 1956.

Wyllie, M.R.J., Gregory, A.R., and Gardner, G.H.F., An experimental investigation of factors affecting elastic wave velocities in porous media: *Geophysics*, 23, 459-493, 1958.

Wyllie, M.R.J., Gardner, G.H.F., and Gregory, A.R., Studies of elastic wave attenuation in porous media: *Geophysics*, 27, 569-589, 1962.

ACKNOWLEDGMENTS

I would like to thank my supervisors, Dr. Ian Stewart and Dr. James Wright, for suggesting the topic of this research and for guidance throughout its development.

I would also like to thank Mike Ryan and Terry White for the fine construction of various parts of the apparatus: and Bob Bradley and Roger Guest for photographs and drafting.

Also I'm grateful to Dr. Noel James of the Dept. of Geology at M.U.N. and geology graduate students George Dix, Mike Ware and Jane Wynne for inspecting the sedimentary cores.

I'd like to thank Ian Baird for drafting the many graphs and Valarie Parsons for patient typing of the manuscript: also Dianne Andrews and Doug Hogan for proofreading the text.

Also I would like to express my gratitude to Memorial University and to the Province of Newfoundland for financial support during part of this research.

Finally, I'm grateful to the Resource Management Branch of the Atlantic Geoscience Centre, Bedford Institute of Oceanography, Dartmouth, N.S. and Petro Canada Exploration Inc. Calgary, for making the core samples available for our use.

